Mohsen AKBARI[1], Seyed Masoud MOGHADDAS-TAFRESHI[2], Masoud ALIAKBAR GOLKAR[3]

K.N. Toosi University of Technology

Wavelet-Based Multi-Resolution Voltage Controller in a Hybrid AC/DC Microgrid

Abstract. *In this paper, a hybrid AC/DCmicrogrid is studied. Furthermore, different control strategies are defined for most of converters in the islanded and grid-connected modes of microgrid to control the voltage of the DC and AC buses. To have a stable operation, converters controller is also coordinated. The main objective of this paper is to design a wavelet-based multi-resolution PI (MRPI) controller for the voltage control of the hybrid microgrid under large disturbances of the study system. The proposed controller is based on the discrete wavelet transform (DWT) of the error signal between actual and command voltages. Results will show more accurate performance of MRPI controller than the conventional PI controller.*

Streszczenie. *W niniejszej pracy, badana jest hybrydowa sieć AC/DC microgrid. Głównym celem niniejszej pracy jest zaprojektowanie falkowej metody sterowania opartej na wielorozdzielczym sterowniku PID (MRPID) sterujący m siecią microgrid w obecności zaburzeń układu i niepewności. Proponowany sterownik bazuje na dyskretnej transformaty falkowej (DWT) sygnału błędu pomiędzy napięciem rzeczywistym a żądanym. Wyniki wykazały dokładniejsze sterowanie kontrolera MRPID w porównaniu z konwencjonalnym regulatorem PI. (**Sterowanie napięciem w sieci microgrid z wykorzystaniem transformaty falkowej**)*

Keywords: hybrid AC/DC microgrid, voltage control, controller, wavelet transform.
Słowa kluczowe: hybrydowy AC / DC microgrid, napięcie sterujące, kontroler, transformaty falkowej.

Introduction

The environmental concerns and electric utility deregulation promote the development of distributed generation (DG) in a rapid pace. The high penetration of DG brings about a concept of the microgrid. It is defined as a cluster of DG units (such as wind turbines and photovoltaics (PVs)), storage devices and loads [1]. The microgrid will separate from the utility and into islanded mode of operation when there are large events like voltage collapses or disturbances in the utility, and intentionally reconnect to the utility while the faults are no longer present [2].

In [3]–[7], AC microgrids have been proposed to facilitate the connection of renewable energy sources to conventional AC systems. However, DC power from some distributed generators, such as PV panels or fuel cells, has to be converted into AC using DC/DC boosters and DC/AC inverters in order to connect to an AC grid. In an AC grid, embedded AC/DC and DC/DC converters are required for various home and office facilities to supply different DC voltages.

Recently, DC microgrids are resurging due to the development and deployment of renewable DC power sources and their inherent advantage for DC loads in commercial, industrial and residential applications [8]–[11]. However, AC sources have to be converted into DC before connected to a DC grid and DC/AC inverters are required for conventional AC loads.

Multiple reverse conversions required in individual AC or DC grids may add additional loss to the system operation and will make the current home and office appliances more complicated [8].

In [12]-[17] hybrid AC/DC microgrids are proposed to reduce processes of multiple reverse conversions in an individual AC or DC microgrid and to facilitate the connection of various renewable AC and DC sources and loads to power system. So in this paper, a hybrid AC/DC microgrid is proposed and studied. Since in all the microgrids, the voltage control is one of the most important issues, so it is also studied in this paper.

Recently, wavelet transforms (WTs) have been used in the modeling, analysis, and control of distributed energy resources for high-performance applications [18]–[22]. The WTs have the ability to decompose wideband signals into time and frequency domains simultaneously in order to focus on short time intervals for high-frequency components and on long time intervals for low frequency components. Khan *et al.* [18] presented wavelet-based multiresolution proportional integral derivative (MRPID) controller for temperature control of the ambient air of battery storage system of the hybrid electric vehicles using two-level discrete wavelet transform (DWT). Song *et al.* [19] presented a multi-resolution modeling approach using wavelet neural networks for a lithium battery model. Also, Xiaojuan *et al.* [20] used wavelet analysis theory for equivalent circuit model of lithium battery aiming at the characteristics of output signal with gaussian white noise when the lithium battery is discharged or charged. The output of current signal and voltage signals in lithium battery are decomposed into multi-scale functions by wavelet base function to realize filter processing of noise signals, and then the filtered signals be reconstructed to obtain more accurate battery resistance. Saleh *et al.* [21] introduced an implementation procedure and performance testings of a WT-based digital protection for microgrid systems. This digital protection is structured for detecting and classifying faults based on the values of the WT coefficients of the high frequency subbands present in the *d*-*q*-axis current components. The WT coefficients are determined using the Daubechies 'db4' wavelet basis functions, which are found optimal for analyzing transient disturbances likely to occur in power systems and electric machines. Also, Shi *et al.* [22] analysed the existed protection of microgrid. In the protection scheme, current traveling waves measured are decomposed by wavelet multi-resolution analysis. The initial traveling waves are compared in magnitude and polarity with each other to determine the faulted feeder.

The main objective of this paper is to develop wavelet-based multiresolution PI (MRPI) controllers for the precise voltage control of the proposed microgrid under large disturbances of the microgrid. The proposed controllers are based on the DWT of the error signal between actual and command voltages. The control signals are generated by wavelet-transformed coefficients of the error signal of different frequency subbands of the DWT after being scaled by their respective gains. The performance of the controllers is evaluated through simulation results. The proposed MRPI controllers are also compared with PSO-optimized fixed-gain PI controllers in simulation. The performances of the proposed MRPI controllers-based

microgrid are found to be more robust and quicker than those of the optimized and fixed-gain controllers based microgrid.

System configuration and resources modeling

Proposed hybrid microgrid configuration

A hybrid microgrid as shown in Fig. 1 is proposed and modeled in MATLAB/Simulink. PV array is connected to DC bus through a DC/DC boost converter to simulate DC sources. A capacitor C_{pv} is used to suppress high frequency ripples of the PV output voltage.

Also, a wind turbine with DFIG is connected to an AC bus to simulate AC sources. In addition, a battery and a super-capacitor (SC) as the energy storages are separately connected to DC bus through bidirectional (buck-boost) DC/DC converters. DC and AC loads are also connected to DC and AC buses, respectively. The DC load was considered as a pure resistive load, but the connected AC load was included constant-impedance (resistance-inductance), constant-capacitance, and constant-power (induction motor) loads. The rated voltages for DC and AC parts are 400 V and 400 V rms, respectively. Furthermore, a 3-phase bidirectional DC/AC main converter with R-L-C filter connects the DC part to the AC part through an isolation transformer.

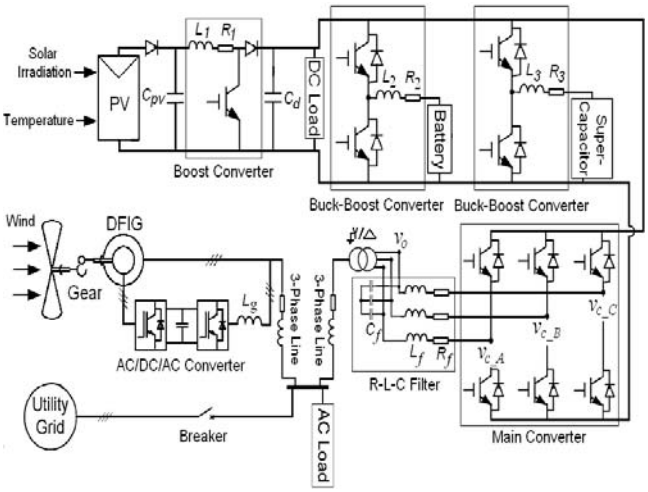

Fig.1. A compact representation of the proposed hybrid microgrid

Modeling of energy resources

Modeling of PV array

Fig. 2 shows an equivalent circuit of a PV panel modeled by a controlled current source. i_{pv} and v_{pv} are terminal current and voltage of the PV panel, respectively. Further, the series resistance (R_s) indicates the losses of the solar cell, while the shunt resistance (R_p) is to represent the reverses current of the diode. However, in this research the R_p will be supposed infinite. Therefore, the current output of the PV panel was modeled by [23]-[24]:

$$I_{pv} = n_p I_{ph} - n_p I_{sat}\left[\exp\left(\left(\frac{q}{AkT}\right)\left(\frac{V_{pv}}{n_s} + I_{pv}R_s\right)\right) - 1\right] \tag{1}$$

$$I_{ph} = \left(I_{sso} + k_i\left(T - T_r\right)\right)\cdot\frac{S}{1000} \tag{2}$$

$$I_{sat} = I_{rr}\left(\frac{T}{T_r}\right)^3 \exp\left(\left(\frac{qE_{gap}}{kA}\right)\cdot\left(\frac{1}{T_r} - \frac{1}{T}\right)\right) \tag{3}$$

Parameters of the 35 kW PV array, used in this study, are shown in Table 1.

Table 1. Parameters of PV array

Symbol	Description	Value
V_{oc}	Rated open circuit voltage	403 V
I_{ph}	Photocurrent	
I_{sat}	Module reverse saturation current	
q	Electron charge	1.602E-19 C
A	Ideality factor	1.5
k	Boltzman constant	1.38E-23 J/K
R_s	Series resistance of a PV cell	
R_p	Shunt resistance of a PV cell	
I_{sso}	Short-circuit current	3.27 A
k_i	SC current temperature coefficient	1.7E-03
T_r	Reference temperature	301.18 K
I_{rr}	Reverse saturation current at T_r	2.0793E-06 A
E_{gap}	Energy of the band gap for silicon	1.1 eV
n_p	Number of cells in parallel	35
n_s	Number of cells in series	900
S	Solar radiation level	0~1000 W/m2
T	Surface temperature of the PV	301.18 K

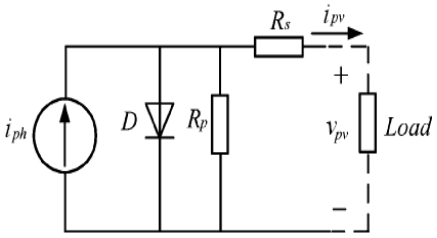

Fig.2. Equivalent circuit of a solar panel

Modeling of battery and SC storages

Although renewable resources are attractive, they are not always dependable in the absence of energy storage devices. The utilization of energy storage units in power systems can be classified into two categories. One is in response to fast transients and the other is related to steady-state energy exchanging. SCs are good candidates for the former application and batteries are suitable for the latter one. Currently, the mixed use of fast and slow energy storage units is gaining popularity for interconnection of renewable generation [25].

In this study, a 50 Ah nickel-metal-hydride (NiMH) battery was used together with an SC storage. The battery was modeled using a controlled nonlinear voltage source in series with a constant resistance [26] as shown in Fig. 3. The controlled voltage source in charging and discharging modes is described by equation:

Charge mode (i^*<0):

$$f_1\left(it, i^*, i, Exp\right) = E_0 - K\cdot\frac{Q}{Q-it}\cdot i^* - K\cdot\frac{Q}{Q-it}\cdot it + Laplace^{-1}\left(\frac{Exp(s)}{Sel(s)}\cdot 0\right) \tag{4}$$

Discharge mode (i^*>0):

$$f_2\left(it, i^*, i, Exp\right) = E_0 - K\cdot\frac{Q}{|it| + 0.1\cdot Q}\cdot i^* - K\cdot\frac{Q}{Q-it}\cdot it + Laplace^{-1}\left(\frac{Exp(s)}{Sel(s)}\cdot\frac{1}{s}\right) \tag{5}$$

where, E_{batt} is nonlinear voltage, E_0 is constant voltage, *Exp(s)* is exponential zone dynamics, *Sel(s)* represents the battery mode (*Sel(s)*=0 during battery discharge, and *Sel(s)*=1 during battery charging), K is polarization constant, i^* is low frequency current dynamics, i is battery current, it is extracted capacity, Q is maximum battery capacity, A is exponential voltage, and B is exponential capacity.

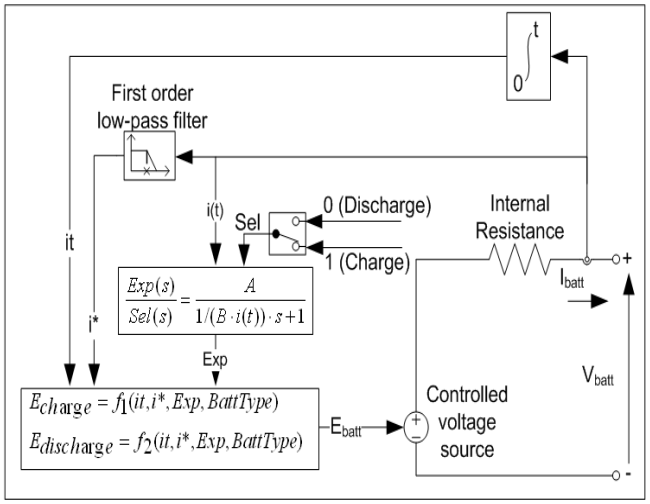

Fig.3. Non-Linear battery model

Also, in modeling of the 5 F super-capacitor storage, it was assumed that it is an ideal capacitance element, i.e. its resistance was exactly considered to zero.

Modeling of wind turbine generator

The stator and rotor voltages of the doubly excited DFIG are supplied by the grid and the power converters, respectively. The mathematical models of a DFIG are essential requirements for its control system. These models are well established in the literature [27], however, for the sake of completeness of the paper, they are introduced in brief later. The voltage equations of an induction motor in a rotating *d–q* coordinate are as follows:

$$\begin{bmatrix} v_{ds} \\ v_{qs} \\ v_{dr} \\ v_{qr} \end{bmatrix} = \begin{bmatrix} -R_s & 0 & 0 & 0 \\ 0 & -R_s & 0 & 0 \\ 0 & 0 & R_r & 0 \\ 0 & 0 & 0 & R_r \end{bmatrix} \begin{bmatrix} i_{ds} \\ i_{qs} \\ i_{dr} \\ i_{qr} \end{bmatrix} + p \begin{bmatrix} \lambda_{ds} \\ \lambda_{qs} \\ \lambda_{dr} \\ \lambda_{qr} \end{bmatrix} + \begin{bmatrix} -\omega_1 \lambda_{qs} \\ \omega_1 \lambda_{ds} \\ -\omega_2 \lambda_{qr} \\ \omega_2 \lambda_{dr} \end{bmatrix} \tag{6}$$

$$\begin{bmatrix} \lambda_{ds} \\ \lambda_{qs} \\ \lambda_{dr} \\ \lambda_{qr} \end{bmatrix} = \begin{bmatrix} -L_s & 0 & L_m & 0 \\ 0 & -L_s & 0 & L_m \\ -L_m & 0 & L_r & 0 \\ 0 & -L_m & 0 & L_r \end{bmatrix} \begin{bmatrix} i_{ds} \\ i_{qs} \\ i_{dr} \\ i_{qr} \end{bmatrix} \tag{7}$$

The dynamic equation of the DFIG

$$\frac{J}{n_p}\frac{d\omega_r}{dt} = T_m - T_{em} \tag{8}$$

$$T_{em} = n_p L_m \left(i_{qs} i_{dr} - i_{ds} i_{qr} \right) \tag{9}$$

where the subscripts *d*, *q*, *s*, and *r* denote *d*-axis, *q*-axis, stator, and rotor respectively, *L* represents the inductance, λ is the flux linkage, *v* and *i* represent voltage and current respectively, ω_1 and ω_2 are the angular synchronous speed and slip speed respectively, $\omega_2=\omega_1-\omega_r$, T_m is the mechanical torque, T_{em} is the electromagnetic torque and other parameters of DIFG are listed in Table 2.

Also, parameters of the converters and isolation transformer are shown in Tables 3 and 4.

Table 2. Parameters of DFIG

Symbol	Description	Value
P_{nom}	Nominal power	45 kW
V_{nom}	Nominal voltage	400 V
L_s	Stator inductance	0.171 pu
R_s	Stator resistance	0.00706 pu
L_r	Rotor inductance	0.156 pu
R_r	Rotor resistance	0.005 pu
L_m	Mutual inductance	2.9 pu
J	Rotor inertial constant	3.1 S
n_{pole}	Number of poles	6
$V_{dc\_nom\_DFIG}$	Nominal DC voltage of AC/DC/AC converter	800 V
P_m	Nominal mechanical power	40 kW

Table 3. Parameters of the converters

Symbol	Description	Value
C_{pv}	Capacitor across the solar panel	110 μF
C_d	Capacitor across the dc-link	8000 μF
L_1	Inductor for the boost converter	2.5 mH
L_2	Inductor for the battery converter	3 mH
R_2	Resistance for the battery converter	0.1 Ω
L_3	Inductor for the SC converter	2 mH
R_3	Resistance for the SC converter	0.07 Ω
L_f	Filtering inductor for the inverter	1.2 mH
R_f	Equivalent resistance of the inverter	0.8 Ω
C_f	Filtering capacitor for the inverter	200 μF
f_s	Switching frequency of converters	12 kHz

Table 4. Parameters of the isolation transformer

Symbol	Description	Value
P_n	Nominal power	50 VA
L_{T_1}	Winding 1 inductance	0.004 pu
R_{T_1}	Winding 1 resistance	0.002 pu
L_{T_2}	Winding 2 inductance	0.004 pu
R_{T_2}	Winding 2 resistance	0.002 pu
L_m	Magnetizing inductance	500 pu
R_m	Magnetizing resistance	500 pu
n_1/n_2	Winding ratio	2:1

Controllers

The hybrid microgrid can operate in two modes: grid-connected mode and islanded mode. In this study system, when the AC part of the microgrid is directly connected to the utility grid, the magnitude of DC part voltage can be regulated by the energy storages located in DC part. And the magnitude and frequency of AC part voltage are the same with the utility grid. However, when the microgrid works in the islanded operation mode, DC part voltage will be regulated by the energy storages located in the DC part, while the magnitude and frequency of AC part are controlled by the parallel inverter (main converter). The controllers used for both operating modes are described in the following sub-sections.

Boost converter controller

The control objective of the boost converter is to track the maximum power point (MPP) of the PV panel. To achieve this objective, P&O method proposed in [28] was used, as shown in Fig. 4.

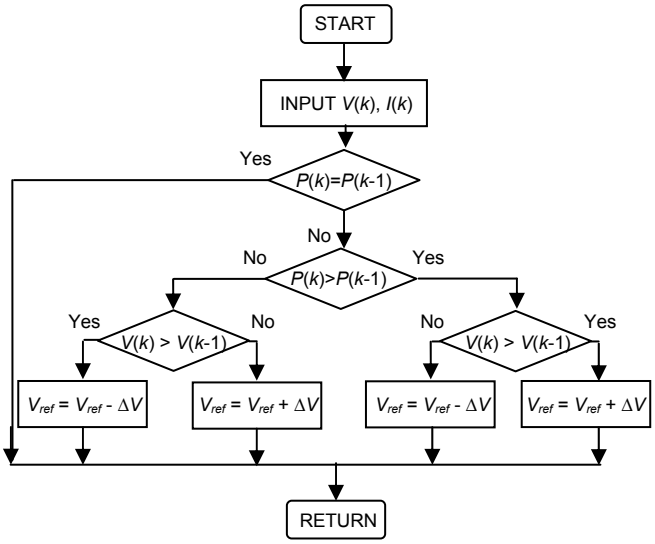

Fig.4. MPPT algorithm for the PV array

Coordinated control scheme of battery and SC storages

Battery has high energy density whereas it has relatively slow charging and discharging speed. On the other hand, SC has high power density and fast response. The mixed use of these energy storage units can make them complimentary to each other. Based on the above characteristics of battery and SC storages, a hybrid control scheme was designed as shown in Fig. 5.

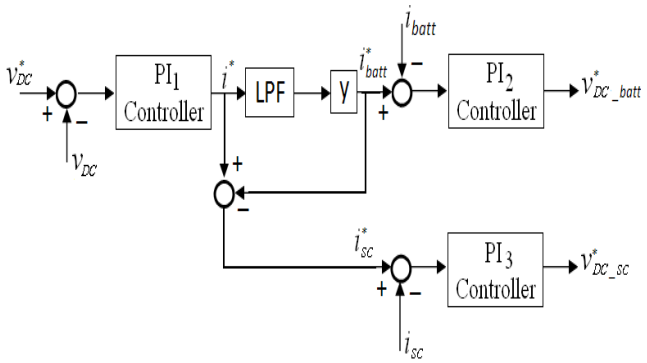

Fig.5. Coordinated control scheme of the battery and SC storages

In this scheme, the DC part voltage is coordinately controlled by battery and SC storages. First, the measured DC part voltage v_{DC} is compared with its reference v^*_{DC} and the difference is sent to a PI controller to get the current reference i^*. Then i^* is split into two parts. One is the battery current reference i^*_{batt} which is obtained by applying a low-pass filter (LPF) with a cut-off frequency 25 Hz and a coefficient y (equal to 0.97 in this study) to i^*. The other one, i^*_{sc}, is the difference between i^* and i^*_{batt}. By this means, the high frequency part of the DC part disturbance and somehow low frequency part will be mitigated by SC and the remained low frequency part of the disturbance is smoothed by battery. The current references i^*_{sc} and i^*_{batt} will be used in the constant current control of the buck-boost converters shown in Fig. 1.

Control scheme of the inverter (main converter)

Grid-connected mode

The main converter can be designed to provide a pre-defined active and reactive power. The proposed control scheme and detailed schematic of the main converter are shown in Figs. 6 and 7, respectively. i^*_{fd} and i^*_{fq} are respectively showing the active and reactive powers, transferring between the DC and AC parts. In this study, i^*_{fd} was considered to zero, while i^*_{fq} was considered to a non-zero value. It means that main converter will just transfer the reactive power between DC and AC buses, when the microgrid is operating in the grid-connected mode.

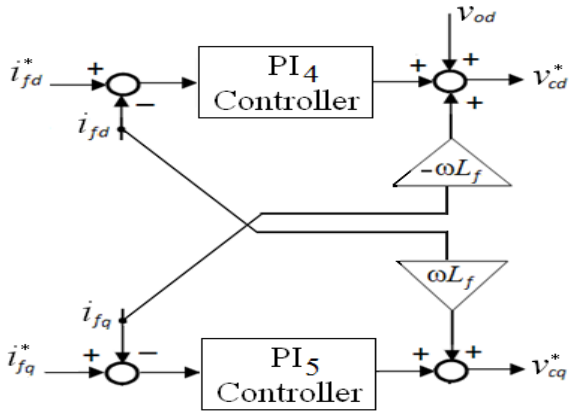

Fig.6. Control scheme of main converter in grid-connected mode

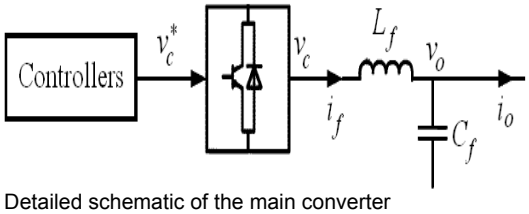

Fig.7. Detailed schematic of the main converter

Islanded mode

When microgrid operates in the islanded mode, the main converter acts as a voltage source to provide a stable voltage and frequency for the AC grid, while the DC grid voltage will be controlled by the battery and SC storages.

Multi-loop voltage control for a DC/AC inverter is described in [29], where the control objective is to provide a high quality AC voltage with good dynamic response at different load conditions. This control scheme was also applied for the main converter to provide high quality AC voltage in the islanded mode, as shown in Fig. 8.

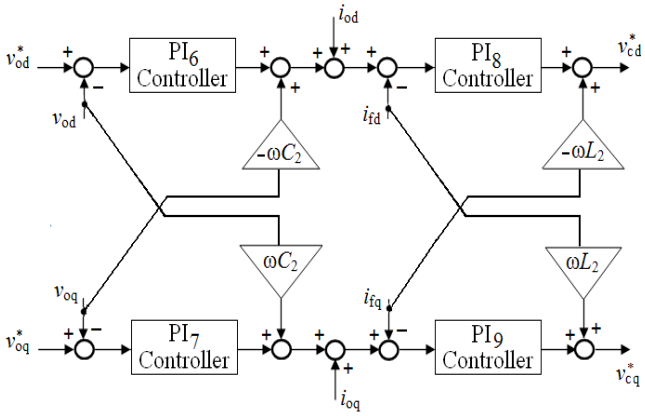

Fig.8. Control scheme of main converter in the islanded mode

DFIG controller

The objectives of the rotor-side converter are to track the MPP of the wind turbine generator and to manage the stator-side reactive power. Different control schemes such as the direct torque control (DTC) and direct power control (DPC) have been proposed for a DFIG in literature [30]-[31]. The DTC scheme as shown in Fig. 9 is selected as the control method for the rotor-side converter in this paper. The rotor rotational speed was obtained through the MPP tracking algorithm, which is based on algorithm proposed in

[32], to track the MPP of wind turbine. ω_r and the mechanical power P_m are used to calculate the electromagnetic torque T^*_{em}. The rotor-side reference *d*-axis current ($i_{dr}^{*\varphi}$) is determined by T^*_{em} and the estimated stator flux linkage (λ_s). In Fig. 9, φ shows the variables in stator voltage oriented reference frame. Also, it is important to say that the reference reactive power Q^*_s was considered to 0.06 pu.

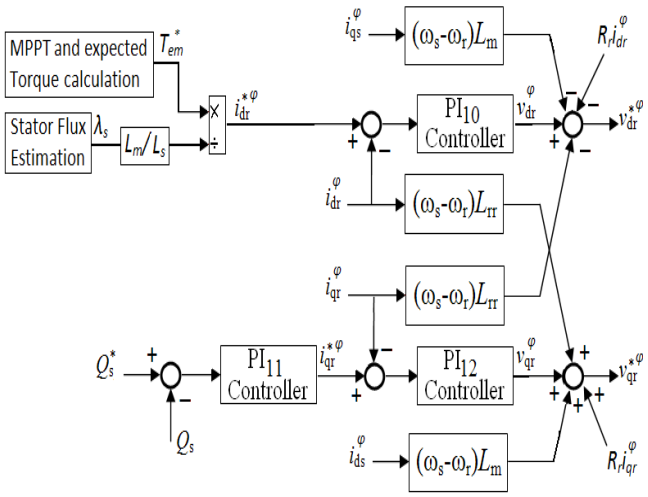

Fig.9. The DTC control scheme for the rotor side converter.

The grid-side converter was designed to regulate the voltage of its own DC-link capacitor. In addition, this model allows using grid-side converter to generate or absorb reactive power. This control system is illustrated in Fig. 10. The voltage of the DC-link is controlled by i_{dg}, while the reactive power is controlled by i_{qg}.

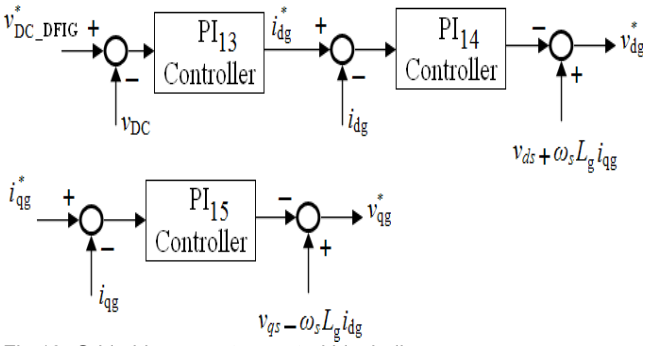

Fig.10. Grid-side converter control block diagram

Multiresolution analysis

The multiresolution analysis (MRA) can extract and localize frequency components of a signal in time [33]-[34]. A simple wavelet-based MRA is constructed through cascaded stages. Each stage has low- and high-pass filters. The down sampling technique separates these stages by two processes to carry out octal frequency dilation. The mother wavelet function determines the coefficients of the low- and high-pass filters of the DWT. A brief introduction of the DWT is provided in [35].

The DWT is a time scale representation of a digital signal using digital filtering techniques. In the DWT, the resolution is changed by filtering operations, and the scale is changed by the downsampling operations [36]. The DWT begins with passing the discrete signal $x[n]$ of length N through a high-pass filter with impulse response $H[n]$ and through a low-pass filter with impulse response $G[n]$. The outputs of the high- and lowpass filters constitute one level of decomposition of the discrete signal. It can be mathematically expressed as [36]:

$$d^1[n] = \sum_{k=0}^{N-1} x[k]H[n-k] \tag{10}$$

$$a^1[n] = \sum_{k=0}^{N-1} x[k]G[n-k] \tag{11}$$

Here, $d^1[n]$ and $a^1[n]$ are outputs of the high- and low-pass filters, respectively. They represent the detail (d^1) and approximation (a^1) of the original signal at level 1. Again, the outputs from the low-pass filter (a^1) can be downsampled by two and then passed through another pair of high- and low-pass filters (identical with the first pair). This constitutes the second level of decomposition of the discrete signal.

The decomposition tree of the DWT up to the second level of resolution, which uses the high-pass (*H*) and low-pass (*G*) filters in the decomposition process, is shown in Fig. 11.

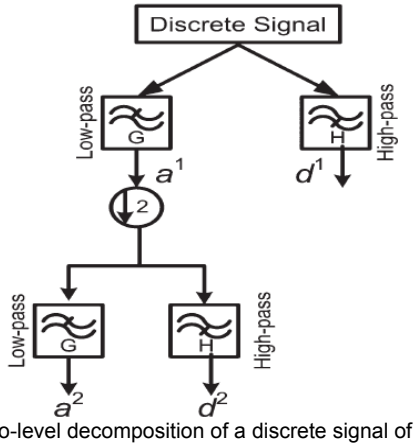

Fig.11. Two-level decomposition of a discrete signal of the DWT

In this study, in DWT-based MRPI voltage controllers, the proportional and integral of the voltage error (*e*) were implemented by the output of the low-pass and high-pass filters of first decomposition level, respectively. A literature survey by authors and past experience show that the mother wavelet 'db4' is the best for short and fast transient disturbances [37]. Therefore in this study, wavelet 'db4' was used to detrmine the coefficients of the high- and low-pass filters of DWT. The DWT-based analysis for the voltage error is shown as below:

$$e_{d^1}[n] = \sum_{k=0}^{N-1} e[k]H[n-k] \tag{12}$$

$$e_{a^1}[n] = \sum_{k=0}^{N-1} e[k]G[n-k] \tag{13}$$

The number of the parameters of the MRPI voltage controllers is dependent on the number of decomposition levels. In this study, as only the first DWT decomposition level was used for the MRPI voltage controllers, so the proposed MRPI voltage controllers include two parameters: k_d^1 and k_a^1, in which k_d^1 is used to tune high-frequencoy components and k_a^1 is used to tune low-frequency components of the voltage error.

In this study, totally three DWT-based voltage controllers were considered. A MRPI controller was considered for the voltage control of the DC bus through battery and super-capacitor storages as shown in Fig.12. In this control scheme, high-frequency and low-frequency components of the WT of the voltage error are scaled by a gain, passed through a saturation limiter and then are used to the current PI controller of the super-capacitor and

battery storages, respectively. Note y_1 and y_2 are respectively correspended with k_d^1 and k_a^1 in above.

Also, two MRPI controllers were considered for the voltage control of the AC bus through the existed inverter as shown in Fig. 13. As shown in Fig. 13, the high-frequency and low-frequency components in the WT of the voltage error are scaled by gains, passed through a saturation limiter, added together, and then they are used in the the current PI controllers. It is important to say that these MRPI controllers of the inverter have the same gains. In other words, the control signal 'u_{MRPI}', is calculated from the detail and aproximation of the voltage error in (12) and (13) as below:

$$u_{MRPI} = y_3 * e_{d1} + y_4 * e_{a1} \tag{14}$$

where y_3 and y_4 are respectively correspended with k_d^1 and k_a^1 in above.

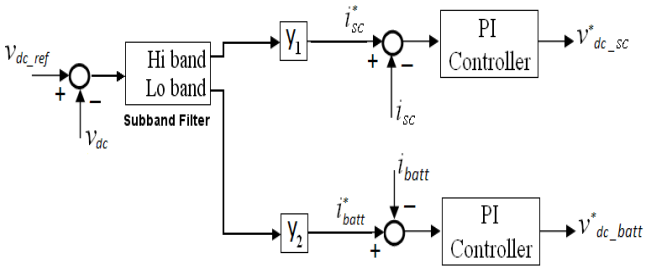

Fig.12. DWT-based controller for super-capacitor and battery storages in order to control the DC bus voltage

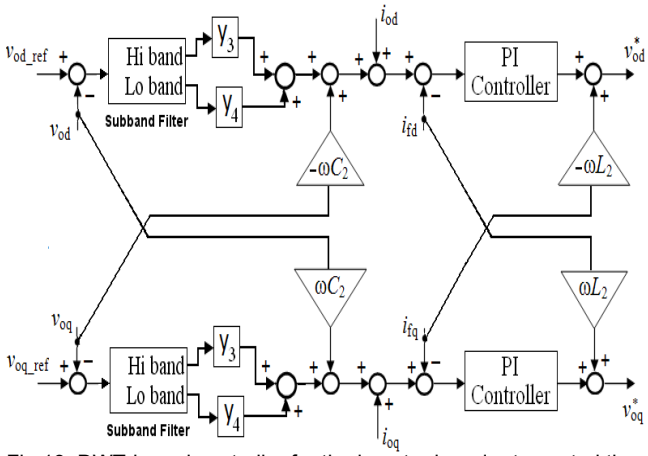

Fig.13. DWT-based controller for the inverter in order to control the AC bus voltage

Dynamic simulations

In this section, simulations performed in MatLab/Simulink are shown to verify the improvement in the voltage control through the MRPI voltage controllers compared to the PI-based voltage controllers. It is important to say that for optimal tuning the PI-based voltage controllers a PSO algorithm was used to optimize their parameters. The voltage and frequency responses of the microgrid under the islanding event occurred in time 0.7 s are shown and compared for both voltage controller types in Figs. 14-16. In this study, two operation conditions were considered: 1) DC load 20 kW and AC load 50 kW, and 2) DC load 20 kW and AC load 30 kW. It can be seen that the wavelet-based controllers are more robustness to quickly control and stablize the voltage and frequency of the hybrid microgrid as compared to the PI-based voltage controllers.

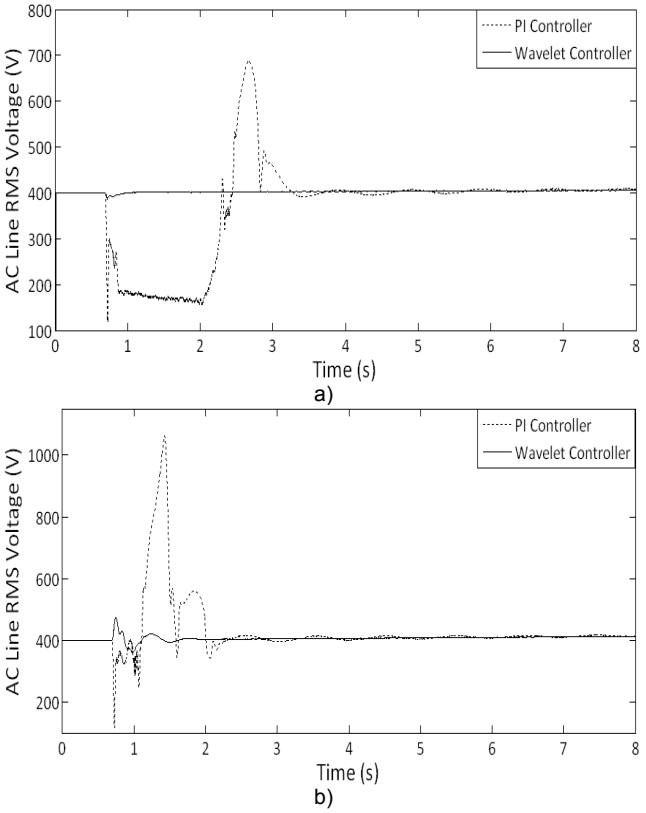

Fig.14. AC bus voltage during the islanding event for the different operation conditions: a) DC load 20 kW and AC load 50 kW, 2) DC load 20 kW and AC load 30 kW

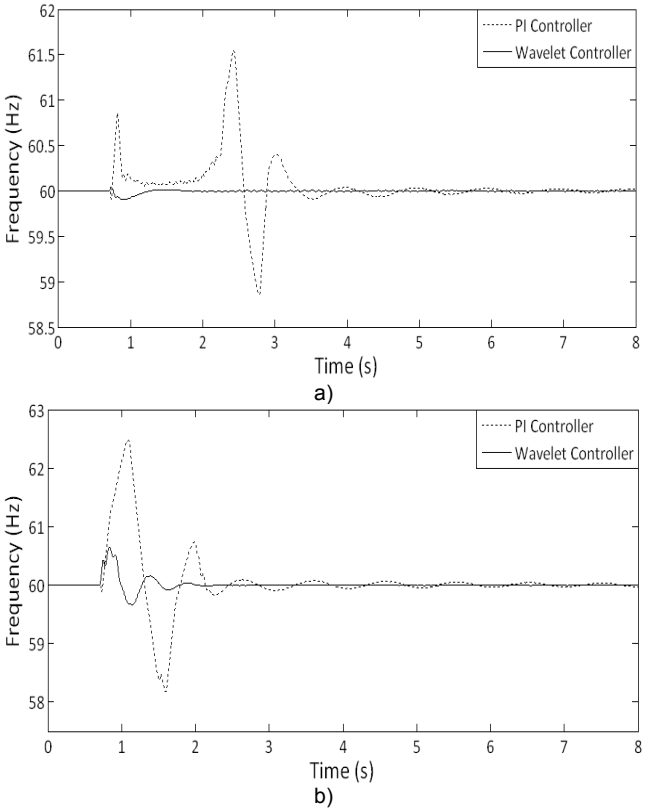

Fig.15. AC bus frequency during the islanding event for the different operation conditions: a) DC load 20 kW and AC load 50 kW, 2) DC load 20 kW and AC load 30 kW

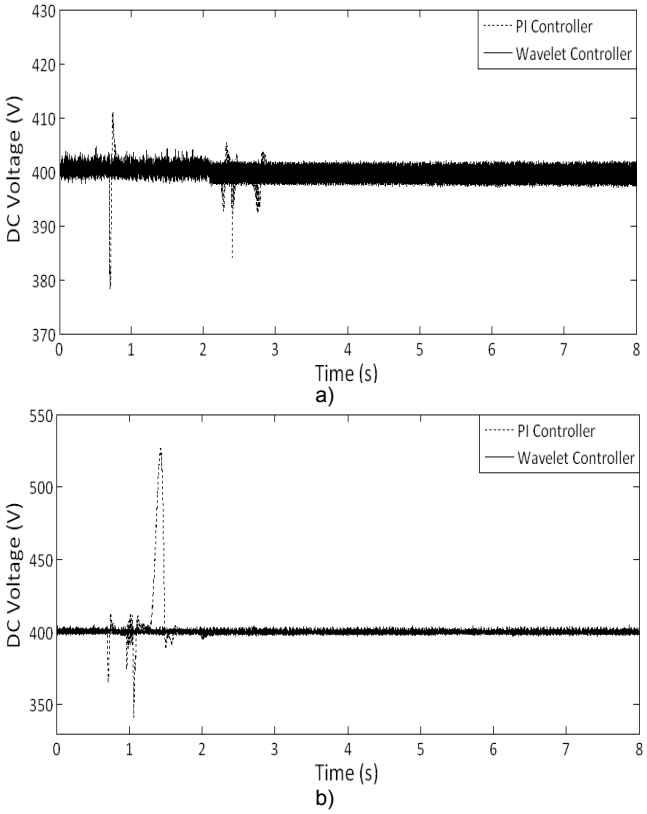

Fig.16. DC bus voltage during the islanding event for the different operation conditions: a) DC load 20 kW and AC load 50 kW, 2) DC load 20 kW and AC load 30 kW

Further, the operation mode change of the microgrid from the islanded mode to the grid-connected mode was studied. The simulation results are shown in Fig. 17 for the operation condition 'DC load 20 kW and AC load 30 kW'. Again, the results show the robustness of the MRPI voltage controllers compared to the PI-based voltage controllers.

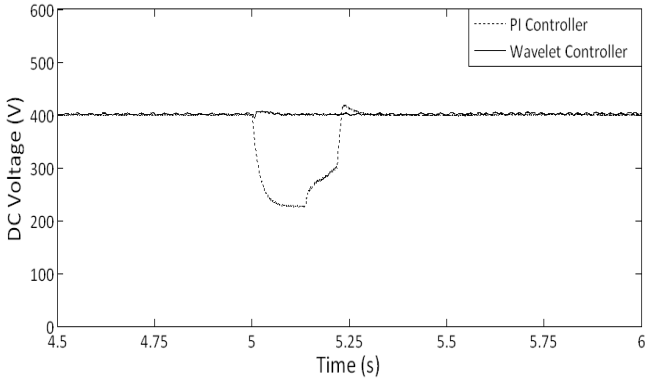

Fig.17. DC bus voltage during the connection of the microgrid to the utility grid

Conclusion

In this paper, the PI controllers among the converters were designed to improve the voltage stability and dynamic voltage control in a hybrid AC/DC microgrid. Then, three DWT-based controllers were designed, modeled and implemented in place of the PI controllers located in the control schemes of the inverter and storages. To have a better response, PI controllers were optimized through the PSO algorithm. Results are achieved during the disconnection from (islanding) and connection to the utility grid, showing that the DWT-based voltage controllers are much more robustness and able to quickly control and stablize the voltage and frequency of the hybrid microgrid as compared to the optimized PI-based voltage controllers.

REFERENCES

[1] Hai-Yan C., Virtual Admittance Based Current Control Strategy for Grid Connected Inverters in Microgrid, *Przegląd Elektrotechniczny*, 87 (2011), No. 12a, 117-120.

[2] Simin P., Gang S., Xu C.Y.C., Control of Different-Rating Battery Energy Storage System Interface to a Microgrid, *Przegląd Elektrotechniczny*, 87 (2011), No. 11, 256-262.

[3] Katiraei F., Iravani M.R., Lehn P.W., Micro-grid Autonomous Operation during and Subsequent to Islanding Process, *IEEE Trans. Power Del.*, 20 (2005), No. 1, 248-257.

[4] Majumder R., Ledwich G., Ghosh A., Chakrabarti S., Zare F., Droop Control of Converter-Interfaced Microsources in Rural Distributed Generation, *IEEE Trans. Power Del.*, 25 (2010), No. 4, 2768-2778.

[5] Delghavi M.B., Yazdani A., Islanded-Mode Control of Electronically Coupled Distributed-Resource Units under Unbalanced and Nonlinear Load Conditions, *IEEE Trans. Power Del.*, 26 (2011), No. 2, 661-673.

[6] Balaguer I.J., Lei Q., Yang S., Supatti U., Peng F.Z., Control for Grid-Connected and Intentional Islanding Operations of Distributed Power Generation, *IEEE Trans. Ind. Electron.*, 58 (2011), No. 1, 147-157.

[7] Wang H., Khambadkone A.M., Yu X., Control of Parallel Connected Power Converters for Low Voltage Microgrid: Part II: Dynamic Electrothermal Modeling, *IEEE Trans. Power Electron.*, 25 (2010), No. 12, 2971-2980.

[8] Salomonsson D., Söder L., Sannino A., An Adaptive Control System for a DC Microgrid for Data Centers, *IEEE Trans. Ind. Appl.*, 44 (2008), No. 6, 1910-1917.

[9] Kakigano H., Miura Y., Ise T., Low Voltage Bipolar Type DC Microgrid for Super High Quality Distribution, *IEEE Trans. Power Electron.*, 25 (2010), No. 12, 3066-3075.

[10] Salomonsson D., Söder L., Sannino A., Protection of Low-Voltage DC Microgrids, *IEEE Trans. Power Del.*, 24 (2009), No. 3, 1045-1053.

[11] Wu T.F., Sun K.H., Kuo C.L., Chang C.H., Predictive Current Controlled 5 kW Single-Phase Bidirectional Inverter with Wide Inductance Variation for DC-Microgrid Applications, *IEEE Trans. Power Electron.*, 25 (2010), No. 12, 3076-3084.

[12] Akbari M., Golkar M.A., Tafreshi S.M.M., A PSO Solution for Improved Voltage Stability of a Hybrid ac-dc Microgrid, *Proc. IEEE PES Innovative Smart Grid Technologies - India (ISGT India)*, Kerala, December 2011, 352-357.

[13] Akbari M., Golkar M.A., Tafreshi S.M.M., Voltage Control of a Hybrid ac/dc Microgrid in Grid-Connected Operation Mode, *Proc. IEEE PES Innovative Smart Grid Technologies - India (ISGT India)*, Kerala, December 2011, 358-362.

[14] Akbari M., Tafreshi S.M.M., Golkar M.A., Voltage Control of a Hybrid ac/dc Microgrid in Stand-Alone Operation Mode, *Proc. IEEE PES Innovative Smart Grid Technologies - India (ISGT India)*, Kerala, December 2011, 363-367.

[15] Jiang Z., Yu X., Power Electronics Interfaces for Hybrid DC and AC-Linked Microgrids, *Proc. IEEE 6th Int. Power Electron. and Motion Control Conf. (IPEMC*), Wuhan, China, May 2009, 730-736.

[16] Bo D., Li Y., Zheng Z., Energy Management of Hybrid DC and AC Bus Linked Microgrid, *Proc. 2nd IEEE Int. Symp. Power Electron. for Distributed Generation Syst. (PEDG)*, Hefei, China, June 2010, 713-716.

[17] Jin C., Loh P.C., Wang P., Mi Y., Blaabjerg F., Autonomous Operation of Hybrid ac-dc Microgrids, *Proc. IEEE Int. Conf. Sustainable Energy Technologies (ICSET)*, Sri Lanka, December 2010, 1-7.

[18] Khan M.A.S.K., Azizur Rahman M., Implementation of Wavelet-Based Controller for Battery Storage System of Hybrid Electric Vehicle, *IEEE Trans. Industry Applications*, 47 (2011), No. 5, 2241-2249.

[19] Song Y., Gao L., Incremental Battery Model Using Wavelet-Based Neural Networks, *IEEE Trans. Components, Packaging and Manufacturing Technology*, 1 (2011), No. 7, 1075-1081.

[20] Xiaojuan H., Xiaojun C., Jianlin L., Dong H., Application of Wavelet Analysis Theory in Storage Energy System of Lithium Battery, *Proc. 2011 30th Chinese Control Conference (CCC)*, Yantai, China, July 2011, 5175-5177.

[21] Saleh S.A., Ahshan R., Rahman M.A., Abu Khaizaran M.S., Alsayed B., Implementing and Testing d-q WPT-Based Digital Protection for Micro-Grid Systems, *Proc. 2011 IEEE Industry Applications Society Annual Meeting (IAS)*, Orlando, FL, USA, October 2011, 1-8.
[22] Shi S., Jiang B., Dong X., Bo Z., Protection of microgrid, *Proc. 10th IET Int. Conf. Developments in Power System Protection (DPSP 2010). Managing the Change*, Manchester, United Kingdom, March/April 2010, 1-4.
[23] Younis M.A., Khatib T., Najeeb M., Mohd Ariffin A., An Improved Maximum Power Point Tracking Controller for PV Systems Using Artificial Neural Network, *Przegląd Elektrotechniczny*, 88 (2012), No. 3b, 116-121.
[24] Khatib T., Mohamed A., A Reliable Maximum Power Point Tracker for Photovoltaic System, *Przegląd Elektrotechniczny*, 88 (2012), No. 2, 145-148.
[25] Garcia F.S., Ferreira A.A., Pomilio J.A., Control Strategy for Battery-Ultracapacitor Hybrid Energy Storage System, *Proc. 24th Annu. IEEE Appl. Power Electron. Conf. and Exposition (APEC)*, Washington, DC, USA, February 2009, 826-832.
[26] Tremblay O., Dessaint L.-A., Dekkiche A.-I., A Generic Battery Model for the Dynamic Simulation of Hybrid Electric Vehicles, *Vehicle Power and Propulsion Conf.*, 2007, 284-289.
[27] Mei F., Pal B.C., Modeling SND Small Signal Analysis of a Grid Connected Doubly Fed Induction Generator, *Proc. IEEE PES Gen. Meeting*, San Francisco, CA, 2005, 358–367.
[28] Khanh L.N., Seo J.-J., Kim Y.-S., Won D.-J., Power Management Strategies for a Grid-Connected PV-FC Hybrid System, *IEEE Trans. Power Deliv.*, 25 (2010), No. 3, 1874-1882.
[29] Pogaku N., Prodanovic M., Green T.C., Modeling, Analysis and Testing of Autonomous Operation of an Inverter-Based Microgrid, *IEEE Trans. Power Electron*., 22 (2007), No. 2, 613-625.
[30] Arnalte S., Burgos J.C., Rodriguez-amenedo J.L., Direct Torque Control of a Doubly-Fed Induction Generator for Variable Speed Wind Turbines, *Elect. Power Compon. Syst.*, 30 (2002), No. 2, 199–216.
[31] Kim W.S., Jou S.T., Lee K.B., Watkins S., Direct Power Control of a Doubly Fed Induction Generator with a Fixed Switching Frequency, *Proc. IEEE Ind. Appl. Soc. Annu. Meeting*, October 2008, 1–9.
[32] Thongam J.S., Ouhrouche M., *MPPT Control Methods in Wind Energy Conversion Systems*, In: Carriveau R., *Fundamental and Advanced Topics in Wind Power*, *InTech-Open Access Publisher*, Croatia, 2011, 339-360.
[33] Shariatinasab R., Akbari M., New Islanding Detection Technique for DG Using Discrete Wavelet Transform, *Proc. IEEE Int. Conf. Power Energy (PECon)*, Kuala Lumpur, Malaysia, 2010, 294-299.
[34] Shariatinasab R., Akbari M., Aghaebrahimi M.R., A Novel Wavelet-Neural Network Method for Fault Location Analysis on Transmission Lines, Presented in *the 16th IEEE Mediterranean Electrotechnical Conf. (MELECON)*, Tunisia, March 2012.
[35] Mallat S.G., A Theory of Multi-Resolution Signal Decomposition, The Wavelet Representation, *IEEE Trans. Pattern Anal. Mach. Intell.*, 11 (1989), No. 7, 674–693.
[36] Stang G., Nguyen T., *Wavelets and Wavelet Filter Banks*. Wellesley, MA: Wellesley-Cambridge Press, 1996.
[37] Shariatinasab R., Akbari M., Rahmani B., *Application of Wavelet Analysis in Power Systems*, In: Baleanu D., *Wavelet Transform/Book 2*, *InTech-Open Access Publisher*, Croatia, under publication.

***Authors**: M. Akbari, dr. S.M. Moghaddas Tafreshi, and prof. M.A. Golkar are with the Electrical and Computer Engineering Department, K.N. Toosi University of Technology.*
E-mail: mohsenakbari@ieee.org, tafreshi@eetd.kntu.ac.ir, masoudgolkar@gmail.com)

The correspondence address is:

e-mail: mohsenakbari@ieee.org
Electrical and Computer Engineering Department, K.N. Toosi University of Technology, P.O. Box: 16315-1355, Tel.: +98 21 468 22096; fax: +98 21 884 62066.